Available online at www.sciencedirect.com
ScienceDirect
International Journal of Heat and Mass Transfer 50 (2007) 3561–3574
International Journal of HEAT and MASS TRANSFER
www.elsevier.com/locate/ijhmt

Laminar conjugate mixed convection in a vertical channel with heat generating components

G. Madhusudhana Rao, G.S.V.L. Narasimham *

Department of Mechanical Engineering, Indian Institute of Science, Bangalore 560 012, India

Received 7 July 2006; received in revised form 10 November 2006
Available online 26 March 2007

Abstract

Conjugate mixed convection arising from protruding heat generating ribs attached to substrates (printed circuit boards) forming channel walls is numerically studied. The substrates with ribs form a series of vertical parallel plate channels. Assuming identical disposition and heat generation of the ribs on each board, a channel with periodic boundary conditions in the transverse direction is considered for analysis. The governing equations are discretised using a control volume approach on a staggered mesh and a pressure correction method is employed for the pressure–velocity coupling. The solid regions are considered as fluid regions with infinite viscosity and the thermal coupling between the solid and fluid regions is taken into account by the harmonic thermal conductivity method. Parametric studies are performed by varying the heat generation based Grashof number in the range 10^4–10^7 and the fan velocity based Reynolds number in the range 0–1500, with air as the working medium. Results are obtained for the velocity and temperature distributions, natural convection induced mass flow rate through the channel, the maximum temperatures in the heat sources and the local Nusselt numbers. The natural convection induced mass flow rate in mixed convection is correlated in terms of the Grashof and Reynolds numbers. In pure natural convection the induced mass flow rate varies as 0.44 power of Grashof number. The maximum dimensionless temperature is correlated in terms of pure natural convection and forced convection inlet velocity asymptotes. For the parameter values considered, the heat transferred to the working fluid via substrate heat conduction is found to account for 41–47% of the heat removal from the ribs.

Keywords: Natural; Forced; Mixed; Convection; Vertical; Channel; Conjugate; Protruding; Heat source

1. Introduction

Since the publication of the classic papers of Graetz [1] on forced convection, Elenbaas [2] on natural convection and Ostrach [3] on mixed convection, the subject of channel convection received much attention as revealed by the excellent reviews of Shah and London [4], Ostrach [5], Raithby and Hollands [6] and Aung [7]. Thermal problems related to the cooling of electronic devices gave impetus to new research in the area of channel convection due to factors like discrete heating, coupling of conduction in the substrate and components with the fluid convection. The practical importance of such problems was emphasized in several reviews, for example, in [8]. Since the subject of the present work is combined free-forced convection in a channel with heat generating protruding heat sources mounted on a substrate, the relevant literature is briefly reviewed here.

Davalath and Bayazitoglu [9] numerically studied the two-dimensional forced convection in a series of channels formed by parallel plates with surface mounted rib-like volumic heat sources for both insulating and conducting substrates. The stacking of parallel plates in the transverse direction was simulated by periodic boundary conditions. Young and Vafai [10] conducted an experimental and numerical study of forced convection from single and multiple (up to five) protruding ribs with isoflux bases attached

* Corresponding author. Tel.: +91 80 22932971; fax: +91 80 23600648.
E-mail address: mecgsvln@mecheng.iisc.ernet.in (G.S.V.L. Narasimham).

0017-9310/$ - see front matter © 2007 Elsevier Ltd. All rights reserved.
doi:10.1016/j.ijheatmasstransfer.2006.12.030

Nomenclature

a	thermal diffusivity ($m^2\ s^{-1}$)
c	specific heat capacity ($J\ kg^{-1}\ K^{-1}$)
g	gravitational acceleration ($m\ s^{-2}$)
Gr	Grashof number, $g\beta\Delta TW_c^3/\nu_f^2$
H	height (m)
n	distance measured normal to the block surface into the fluid (also exponent in the correlation for $v_{in,nc}$) (m)
Nu	Nusselt number
p	excess pressure over the hydrostatic (Pa)
Pr	Prandtl number, ν_f/a_f
$\dot{q}$	heat flux ($W\ m^{-2}$)
$\dot{Q}_L$	heat generation rate per unit length of heater perpendicular to the x–y plane ($W\ m^{-1}$)
R^2	multiple correlation, 1 − mean square error/variance
Re	Reynolds number, $(v_{in,fc}W_c)/\nu_f$
s	distance along solid–fluid interface (m)
t	time (s)
T	temperature (°C)
u, v	velocity components in x- and y-directions $m\ s^{-1}$
W	width (m)
x, y	Cartesian coordinates (m)

Greek symbols

α	heat transfer coefficient ($W\ m^{-2}\ K^{-1}$)
β	volumetric expansion coefficient of the fluid (K^{-1})
δ	function with value unity in heat generating region and zero in other regions
ΔT	characteristic temperature difference, $\dot{Q}_L/\lambda_f$ (K)
λ	thermal conductivity ($W\ m^{-1}\ K^{-1}$)
ν	kinematic viscosity ($m^2\ s^{-1}$)
ρ	density ($kg\ m^{-3}$)
ψ	stream function ($m^2\ s^{-1}$)

Subscripts

a,l	average, left
a,r	average, right
c	channel
f	fluid
fc	forced convection
h	heater
in	inlet
l,l	local, left
l,r	local, right
L	per unit length of block
max	maximum
nc	natural convection component in mixed convection
pnc	pure natural convection
p	package (or constant pressure)
ref	reference quantity
s	substrate
w	solid (substrate, package or heater)

Superscripts

*,+	dimensionless quantity

to one wall of a rectangular duct and obtained correlations for Nusselt number. Their results also show that by proper placement of taller ribs, the heat transfer from the ribs in the downstream vicinity can be enhanced. Wang and Saulnier [11] studied the conjugate forced convection heat transfer in a two-dimensional channel constituted by two PCBs with four uniformly heated integrated circuits for steady-state conditions and reported the effect of the thermal conductivity of the substrate and package materials on the fluid and heat flow fields. Developing flow and heat transfer results of Kim and Anand [12] for a similar geometry with cyclic conditions in the transverse direction show that periodically developed (PD) conditions can exist in a channel with five modules for lower Reynolds numbers, higher channel widths and rib spacings and that even a lower thermal conductivity substrate can effectively redistribute the heat and reduce the block temperatures. Kim and Anand [13] reported the results for the same problem with the assumption of PD conditions as they can lead to acceptable, though conservative, block temperature estimates with reasonable computational costs. Asako and Faghri [14] reported three-dimensional computational results for forced convection from block-like components heated by thin heaters mounted on an insulated substrate assuming PD conditions in the streamwise direction. Comparison with two-dimensional results of rib-like components for axial flow and cross-flow reveals that two-dimensional computations can have good predictive capability in some parameter ranges.

Natural and mixed convection studies that take into account the heat conduction in the protruding sources and the substrate received relatively less attention for both plate and channel geometries.

Natural convection from a vertical plexiglass surface with eight stainless steel protrusions heated with foil heaters was experimentally investigated by Joshi et al. [15] with water as the working medium. Wang et al. [16] studied the laminar natural convection air-cooling of five wall-attached protruding, discretely heated integrated circuit packages attached to a vertical substrate and reported the

effects of substrate and component conduction on natural convection.

The numerical study on horizontal and vertical channels performed by Kim et al. [17] considers mixed convection with three heated modules and cyclic conditions in the direction perpendicular to the substrate. This geometry resembles that considered by Davalath and Bayazitoglu [9] for forced convection and Wang and Saulnier [11] for natural convection. Kim et al. [17] report that the cooling efficiency of vertical channels is slightly better than that in horizontal channels and that simple isothermal or adiabatic conditions for the substrate are not adequate to model real systems. The results of a numerical study on laminar mixed convection in a vertical channel with periodic boundary conditions in the transverse direction and with foil-like discrete heaters were reported by Watson et al. [18] taking into account the substrate heat conduction. Najam et al. [19] applied PD conditions for mixed convection in a horizontal channel with protruding isothermal blocks and found that an unsteady flow results because of the interaction of natural convection cells with streamwise flow. Rao et al. [20] investigated the interaction of surface radiation with mixed convection in a vertical channel. The natural convection component was driven by symmetrically deployed discrete volumic heat sources in the channels walls. The sources span the full thickness of the wall. The wall heat conduction coupling was treated as a boundary condition with a fin-type equation and heat transfer correlations were obtained from computational results covering a wide parametric space. Representative papers aimed at the enhancement of mixed convection heat transfer are those of Sultan [21] and Wang and Jaluria [22].

Braaten and Patankar [23] studied the laminar mixed convection from block-like electronic components mounted on the bottom or top wall of a horizontal channel invoking PD conditions in the streamwise direction and treating the channel walls as insulating or perfectly conducting. Their study reveals that buoyancy enhances the forced convection heat transfer with a slight increase in the pressure drop and that the bottom-wall mounting of blocks and the use of higher Prandtl number fluids is desirable for better cooling efficiency of the devices. Sultan [21] experimentally studied the mixed convection cooling enhancement of three isoflux ribs attached to the bottom wall of a horizontal channel by inducted air flow through perforations made in the channel wall portion. At lower Reynolds number, the second heater from the inlet side showed the highest temperature, while at higher Reynolds number, the average temperatures of the heaters were in ascending order. The flow through perforations are found to enhance the heat transfer by about 33%. Wang and Jaluria [22] examined the effect of a vortex promoter placed between the horizontal walls of a channel on the mixed convection heat transfer of two downstream protruding isothermal blocks using a two-dimensional model and report enhanced heat transfer due to resonant effect.

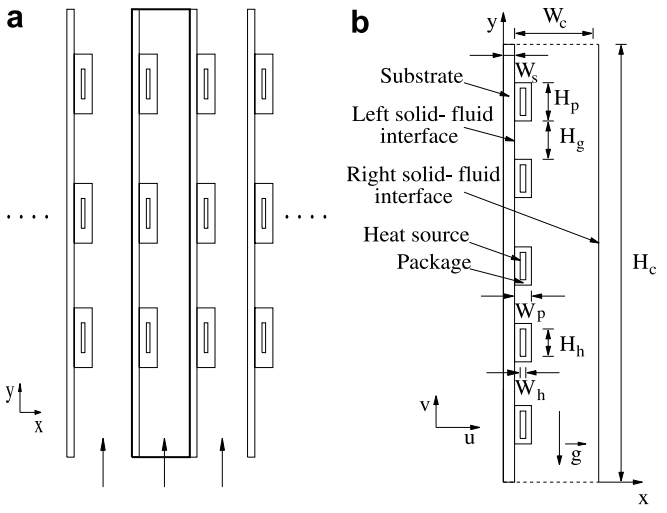

Fig. 1. (a) Geometric configuration; (b) physical model and coordinate system.

2. Physical model and coordinate system

The physical model (Fig. 1) consists of a series of vertical substrates with equal spacing and identical disposition of ribs having the same volumetric heat generation. The ribs are representative of discrete electronic packages densely packed in the third direction. Neglecting the end effects, a series of channels with identical, two-dimensional, flow and temperature distributions can be envisioned. One such channel, consisting of a substrate with sources and the back surface of the following substrate is considered for the analysis. In view of the periodicity in the transverse direction, periodic thermal boundary conditions are applied on the vertical surfaces of the selected domain. An electronic package consists of a thin silicon wafer mounted on a substrate which is sandwiched between epoxy or ceramic covers. Hence the volumetric heat generation in the present study is accounted for in the wafer portion rather than in the entire package. The objectives of the work are to find the temperature and velocity distributions inside the channel and to determine several quantities of interest such as the natural convection induced mass flow rate, maximum dimensionless temperatures of the heat sources and the local and average Nusselt numbers. In the computational domain, there are two solid–fluid interfaces. The stepped interface is referred to as the left solid–fluid interface and the scheme of measuring the distance along this interface is from the location with letter symbol 'a' to the location with the symbol 'v', as shown in Fig. 2. The straight interface, where the fluid comes in contact with the substrate only, is referred to as the right solid–fluid interface.

3. Mathematical formulation

3.1. Governing equations

The flow and temperature distributions are governed by continuity, Navier–Stokes and fluid and solid energy

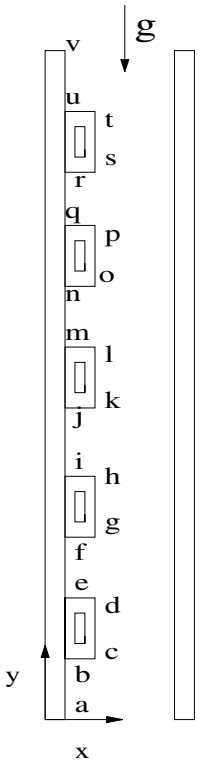

Fig. 2. Measurement of distance along the left solid–fluid interface of the channel.

equations. The radiative heat transfer, viscous heat dissipation and compressibility effects of air are considered to be negligible. The effect of the density variation causing buoyancy force is taken into account through the Boussinésq approximation. The thermophysical properties of the fluid and the solid regions are assumed to be independent of temperature.

The governing equations in dimensionless form read:

$$\frac{\partial u^*}{\partial x^*}+\frac{\partial v^*}{\partial y^*}=0 \tag{1}$$

$$\frac{\partial u^*}{\partial t^*}+u^*\frac{\partial u^*}{\partial x^*}+v^*\frac{\partial u^*}{\partial y^*}=-\frac{\partial p^*}{\partial x^*}+\left(\frac{\partial^2 u^*}{\partial x^{*2}}+\frac{\partial^2 u^*}{\partial y^{*2}}\right) \tag{2}$$

$$\frac{\partial v^*}{\partial t^*}+u^*\frac{\partial v^*}{\partial x^*}+v^*\frac{\partial v^*}{\partial y^*}=-\frac{\partial p^*}{\partial y^*}+\left(\frac{\partial^2 v^*}{\partial x^{*2}}+\frac{\partial^2 v^*}{\partial y^{*2}}\right)+GrT_{\mathrm{f}}^* \tag{3}$$

$$\frac{\partial T_{\mathrm{f}}^*}{\partial t^*}+u^*\frac{\partial T_{\mathrm{f}}^*}{\partial x^*}+v^*\frac{\partial T_{\mathrm{f}}^*}{\partial y^*}=\frac{1}{Pr}\left(\frac{\partial^2 T_{\mathrm{f}}^*}{\partial x^{*2}}+\frac{\partial^2 T_{\mathrm{f}}^*}{\partial y^{*2}}\right) \tag{4}$$

$$\rho_{\mathrm{w}}^* c_{\mathrm{w}}^*\frac{\partial T_{\mathrm{w}}^*}{\partial t^*}=\frac{\lambda_{\mathrm{w}}^*}{Pr}\left(\frac{\partial^2 T_{\mathrm{w}}^*}{\partial x^{*2}}+\frac{\partial^2 T_{\mathrm{w}}^*}{\partial y^{*2}}\right)+\frac{\delta(x^*,y^*)}{Pr} \tag{5}$$

The definitions of the various quantities appearing in the above equations are as follows:

$$x^*=\frac{x}{W_{\mathrm{c}}},\quad y^*=\frac{y}{W_{\mathrm{c}}},\quad t^*=\frac{tv_{\mathrm{f}}}{W_{\mathrm{c}}^2},\quad u^*=\frac{uW_{\mathrm{c}}}{v_{\mathrm{f}}},\quad v^*=\frac{vW_{\mathrm{c}}}{v_{\mathrm{f}}},$$

$$p^*=\frac{pW_{\mathrm{c}}^2}{\rho_{\mathrm{f}}v_{\mathrm{f}}^2},\quad T^*=\frac{T-T_{\mathrm{f,in}}}{\Delta T},\quad \rho_{\mathrm{w}}^*=\frac{\rho_{\mathrm{w}}}{\rho_{\mathrm{f}}},\quad c_{\mathrm{w}}^*=\frac{c_{\mathrm{w}}}{c_{\mathrm{p,f}}},$$

$$\lambda_{\mathrm{w}}^*=\frac{\lambda_{\mathrm{w}}}{\lambda_{\mathrm{f}}},\quad Pr=\frac{v_{\mathrm{f}}}{a_{\mathrm{f}}},\quad Gr=\frac{g\beta\Delta TW_{\mathrm{c}}^3}{v_{\mathrm{f}}^2},\quad \Delta T=\frac{\dot{Q}_{\mathrm{L}}}{\lambda_{\mathrm{f}}}$$

The subscript "w" denotes solid region (i.e., substrate, package or heater). The first four equations in the above set are respectively the continuity, x- momentum, y- momentum and the energy equations, while the last equation is the energy equation for the solid regions. The dimensionless heat generation term is set to zero in the substrate and in the regions of the package other than the silicon wafer through the spatial function $\delta(x^*,y^*)$.

In mixed convection, the dimensionless inlet velocity v_{in}^* is treated as the sum of the forced and the natural convection component (in the presence of mixed convection):

$$v_{\mathrm{in}}^*=Re+v_{\mathrm{in,nc}}^* \tag{6}$$

where Re is based on the fan velocity component. In the pure natural convection case, Re is zero and v_{in}^* becomes $v_{\mathrm{in,pnc}}^*$. It may be noted that if Re is based on the total inlet velocity, it would be non-zero even in pure natural convection and it would be difficult to distinguish between the different regimes. In order to delineate the forced and free convection velocity components, the following approximation is made.

In pure natural convection, the flow is driven by buoyancy with zero net pressure drop between the channel outlet and the inlet, neglecting any pressure defects that may occur at the inlet and the outlet. The same is assumed to be true for the natural convection component in mixed convection. Thus any pressure drop produced in mixed convection is that of the forced convection for the corresponding Re. To proceed with the solution, first the pure forced convection problem with $v_{\mathrm{in}}^*=Re$ and $Gr=0$ is solved for various values of Re and a correlation is established between pressure drop Δp^* and Re. The mixed convection problem is then solved for a prescribed dimensionless total inlet velocity v_{in}^* and Gr, and the pressure drop Δp^* is determined. Since by assumption, the mixed and forced convection pressure drops are the same for a given Reynolds number, the value of Re in mixed convection can be found using the forced convection correlation relating the pressure drop and the Reynolds number. The quantity $v_{\mathrm{in,nc}}^*$ (denoting the dimensionless average natural convection inlet velocity in the mixed convection case) is determined by subtraction, i.e., $v_{\mathrm{in,nc}}^*=v_{\mathrm{in}}^*-Re$. In other words, $v_{\mathrm{in,nc}}^*$ in mixed convection is treated as the additional contribution to the total inlet velocity occurring with zero overall pressure drop over that of the forced velocity component Re resulting from the pressure drop. For $Re=0$ and a given Gr, the dimensionless pure natural convection inlet velocity $v_{\mathrm{in,pnc}}^*$ is separately determined by solving the natural convection problem with equal pressure values at the inlet and the outlet. For the same value of Gr, the mixed and pure natural convection quantities $v_{\mathrm{in,nc}}^*$ and $v_{\mathrm{in,pnc}}^*$ are not the same because of the differing temperature distributions in mixed convection and pure natural convection for the same Gr. Moreover, $v_{\mathrm{in,nc}}^*$ does not necessarily belong to that pure natural convection operating individually (i.e., without simultaneous interaction with the forced flow), with zero overall pressure drop and with the same

temperature field produced by mixed convection. It may be noted that Dalbert [24] earlier distinguished the combined and natural convection régimes in vertical channels based on finite and zero overall channel pressure drop.

3.2. Boundary and initial conditions

The common boundary conditions for the forced, free and combined convection cases are the no slip and mass impermeability conditions at the solid boundaries, periodic (or cyclic or repeated) conditions for the temperature on the left and right boundaries of the computational domain, insulated condition across the thickness of the substrate at the entrance and exit sections, no temperature jump and flux continuity at the solid–fluid boundaries. For the temperature at the exit of the channel, Shyy [25] suggests zero streamwise first derivative while Kennedy and Zebib [26] suggest zero streamwise second derivative, as less restrictive boundary condition, respectively. In the present work, the former condition is used. A uniform temperature of the fluid is prescribed at the inlet of the channel. The periodic temperature conditions across the channel at any dimensionless time can be mathematically stated as follows:

$$\begin{aligned} T^*(x^*,y^*) &= T^*\left(x^*+1+W_s^*,y^*\right) = T^*\left(x^*+2+2W_s^*,y^*\right)\cdots \\ &= T^*\left(x^*-1-W_s^*,y^*\right) = T^*\left(x^*-2-2W_s^*,y^*\right)\cdots \\ &\left[0\leqslant x^*\leqslant\left(1+W_s^*\right),\ \ 0\leqslant y^*\leqslant H_c^*\right] \end{aligned} \tag{7}$$

For forced convection, uniform streamwise velocity and zero cross-stream velocity at the inlet, the pressure at the exit and zero cross-stream velocity gradient in the streamwise direction at the exit are prescribed. The streamwise velocity at the exit is determined using the continuity constraint. These conditions enable the pressure drop to be determined. For natural and mixed convection cases, the pressure drop between the entrance and exit of the channel is prescribed, with the channel exit pressure fixed at zero. The gradient of the cross-stream velocity in the streamwise direction is set to zero at the entrance and exit of the channel. The streamwise velocity at the inlet and exit of the channel is determined using the continuity constraint, imposing the additional condition that the velocity profile at the inlet to channel is rectangular.

The initial conditions are a quiescent state and a uniform temperature throughout the domain. The steady-state solutions are large time solutions obtained by time-marching.

3.3. Nusselt numbers

The left solid–fluid interface consists of substrate portions and three faces of each package. The local heat transfer coefficient at any location on the left interface, $\alpha_{l,l}$ is defined as

$$\alpha_{l,l}(T_{l,l}-T_{in}) \equiv \dot{q}_{l,l} = -\lambda_f\left(\frac{\partial T}{\partial n}\right)_{l,l} \tag{8}$$

where $\dot{q}_{l,l}$ is the local heat flux and n is the distance measured normal to the block surface into the fluid. The local Nusselt number is given by

$$Nu_{l,l} = -\frac{W_c}{T_{l,l}-T_{in}}\left(\frac{\partial T}{\partial n}\right)_{l,l} = \frac{\dot{q}_{l,l}W_c}{\lambda_f(T_{l,l}-T_{in})} = \frac{\dot{q}^*_{l,l}}{T^*_{l,l}} \tag{9}$$

where $\dot{q}^*_{l,l}$ $[=(\dot{q}_{l,l}W_c)/\dot{Q}_L]$ is the dimensionless local heat flux. The local Nusselt number $Nu_{l,r}$ on the fluid–solid interface forming the right boundary of the computational domain is similarly defined.

The average Nusselt numbers $Nu_{a,l}$ and $Nu_{a,r}$ on the left and right solid–fluid interfaces are defined based on the maximum temperature of the warmest heater, which is the heater near the channel exit. For example

$$Nu_{a,l} \equiv \frac{\alpha_{a,l}W_c}{\lambda_f} = -\frac{1}{T^*_{max}}\int\left(\frac{\partial T^*}{\partial n^*}\right)_{l,l} ds^*_l \tag{10}$$

where the limits for the left interface distance s^*_l in the integral are zero and the total interface length. The average Nusselt number $Nu_{a,r}$ is defined in a similar manner.

3.4. Solution methodology

The common objective of the various numerical schemes based on primitive variable equations is to find a pressure field which leads to the satisfaction of continuity equation. The SIMPLE (Semi-Implicit Method for Pressure Linked Equations) algorithm has been adopted for the pressure–velocity coupling. In this procedure, a pressure correction equation is solved in lieu of the continuity equation. The transient term is discretised using backward difference and the combined convective and diffusive terms are discretised with the Power-law scheme on a staggered mesh. An iterative time advancement implicit method is adopted in which the calculation at each time step involves sufficient number of outer iterations on the set of equations. During each outer iteration, the governing equations are again iteratively solved in a sequence. The method is described in detail in [27]. The solution is obtained by vertical sweeps and the well-known tri-diagonal matrix algorithm is used as the equation solver. For the solution of temperature, the cyclic tri-diagonal matrix algorithm, which takes into account the cyclic or repeated conditions in the transverse direction, is employed. The solid is considered as a fluid of infinite viscosity and appropriate thermal conductivity. The thermal coupling at the interface between the solid and fluid regions is taken into account by the harmonic mean thermal conductivity method. Although the interest lies in steady-state solutions, the time-dependent formulation is used for enhanced stability of the algorithm. In order to accelerate convergence to steady state, a false transient approach is adopted by setting the dimensionless thermal capacitance of the solid to unity. Boundary conditions are set via an extra layer of pseudo-cells.

3.5. Validation of the computer program

A computer program is developed to solve the conjugate channel convection problem described above. In order to validate the computer program, the results for buoyancy-driven natural convection flow in a differentially heated cavity and conjugate forced convection in a horizontal channel with periodic boundary conditions in the cross-stream direction are reproduced by modifying the present computer code. The results for the differentially heated cavity are compared with the finite difference [28] and finite element [29] benchmark solutions in Table 1. Fig. 3 compares the isotherm map presented by Davalath and Bayazitoglu [9], for horizontal channel mixed convection with conducting plates of thermal conductivity ratio 10, dimensionless block spacing 0.5, Reynolds number 750 and Prandtl number 0.7 with the isotherm map obtained with the present code for the same problem. It can be seen that there is a favourable agreement between the present and published results for both the problems. Although not shown here, the program is also validated against the results of mixed convection in a channel with discrete heat sources [30]. Kim et al. [17] assumed the silicon wafer in the package to be a planar heat source, which is best described by a heat generating interface from which heat is conducted to either side. However, the authors describe the heat source by including a Dirac delta function type spike in the source term of the energy equation. It appears therefore that the total heat generated depends upon the width of the layer of computational cells approximating the silicon wafer. The exact numerical artefact for accommodating a planar source with a volumetric source in the energy equation is not clear. When an attempt was made to reproduce the results of Kim et al. by treating the silicon wafer as a volumetric source of finite width, there was a good qualitative agreement between the two sets of results.

Table 1
Comparison of the average hot wall Nusselt numbers from the present code for the differentially heated square cavity problem with benchmark solutions

Gr	Present	Reference [28]	% Difference	Reference [29]	% Difference
10^3	1.118	1.117	0.09	1.117	0.09
10^4	2.245	2.238	0.31	2.254	−0.40
10^5	4.509	4.509	0.0	4.598	−1.93
10^6	8.840	8.817	0.26	8.976	−1.51
10^7	16.845	–	–	16.656	1.13
10^8	32.019	–	–	31.486	1.69

3.6. Grid sensitivity tests

In order to select the grid sizes which yield reasonably accurate predictions, grid sensitivity tests are conducted with $Re = 1200$ for forced convection and with $Re = 1200$ and $Gr = 5 \times 10^6$ for mixed convection. In choosing the grids for grid independence study, the number of control volumes for successive grids are increased roughly by a factor of 1.5 in each direction. The results of the grid variation study are presented in Table 2, based on the results of which the 45×259 grid is adopted for the parametric studies. This grid has 45 control volumes in the x^*-direction and 259 control volumes in the y^*-direction. The distribution of the grid points (without the extra layer of pseudo-cells) is shown in Fig. 4, where the continuous lines are the control volume faces.

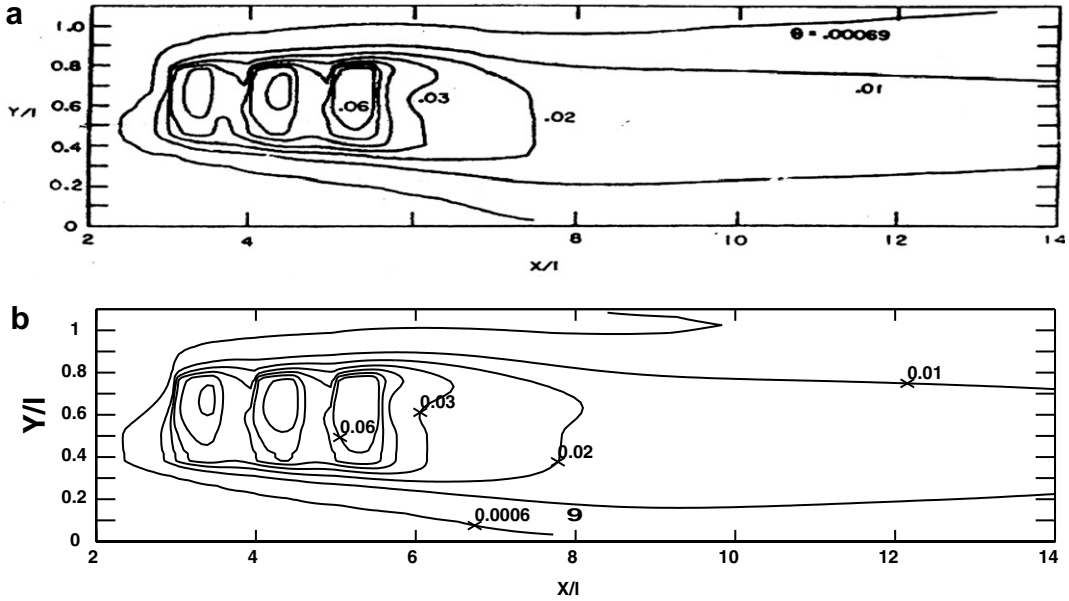

Fig. 3. Comparison of the isotherm map of Davalath and Bayazitoglu [9] (a) for conjugate forced convection in a horizontal channel (conductivity ratio 10, dimensionless block spacing 0.5, Reynolds number 750 and Prandtl number 0.7) with that obtained from the present code (b).

Table 2
Sensitivity of the results for varying grids

Grid size	Pure forced convection (FC)		Mixed convection (MC)	
	$Re = 1200$		$Re = 1200$	$Gr = 5 \times 10^6$
	$T^*_{max} \times 10^2$	$Nu_{a,r}$	$T^*_{max} \times 10^2$	$Nu_{a,r}$
30×175	5.2969	3.6510	5.0441	3.7855
30×259	5.2864	3.6386	5.0145	3.7823
30×390	5.2784	3.6404	4.9972	3.7902
45×175	5.2842	3.6842	5.0306	3.8341
45×259	5.2715	3.6739	4.9971	3.8346
45×390	5.2612	3.6736	4.9765	3.8386
68×175	5.2678	3.7187	5.0098	3.8842
68×259	5.2523	3.7094	4.9730	3.8875
68×390	5.2391	3.7078	4.9487	3.8941

4. Results and discussion

The geometric parameters and physical properties are chosen as $H_c = 170$ mm, $H_g = 15$ mm, $H_p = 15$ mm, $W_c = 15$ mm, $W_p = 5$ mm and $W_s = 2$ mm [11]. The thermal conductivity of the package material ranges from 1 W m^{-1} K^{-1} (plastic type) to 20 W m^{-1} K^{-1} (ceramic type) while that of the substrate varies from 0.1 W m^{-1} K^{-1} (badly conductive epoxy) to 100 W m^{-1} K^{-1} (metallic core type). In the present study the least conductive materials for the package (or integrated circuit) and the substrate are chosen by taking the thermal conductivities as 0.1 W m^{-1} K^{-1} and 1 W m^{-1} K^{-1}, respectively, in order to obtain conservative estimates for the maximum temperatures. Air is chosen as working medium ($Pr = 0.7$). The dimensionless values of the geometric parameters are $H^*_c = 11$, $H^*_g = 1$, $H^*_p = 1$, $W^*_c = 1$, $W^*_p = 0.333$ and $W^*_s = 0.133$. The thermal conductivity ratios for the package and substrate are $\lambda^*_p = 40$ and $\lambda^*_s = 4$. The heat source is the silicon wafer centrally located in the package with a thickness and height respectively one-fifth and one-third of the package. Hence $H^*_h = 0.333$ and $W^*_h = 0.0667$. Since the integrated circuit occupies a very small fraction of the total package volume, the thermal conductivity λ^*_h of the heat source is assumed to be the same as that of the packaging material, i.e., $\lambda^*_h = 40$. The heights of the bottom and top substrate regions (ab and uv in Fig. 2) are taken equal to the inter-block spacing.

The values of the dimensionless pressure drop across the channel in forced convection are presented in Table 3.

4.1. Natural convection induced velocity in the presence of mixed convection

The natural convection induced velocity $v^*_{in,nc}$ in mixed convection is plotted against the Reynolds number $Re(= v_{in,fc} W_c/\nu_f)$ in Fig. 5 for various values of the Grashof number. The values of $v^*_{in,nc}$ for $Re = 0$ correspond to the pure natural convection case. It can be seen that at a given Grashof number the quantity $v^*_{in,nc}$ decreases with increasing Reynolds number. This decrease is due to better cooling of the components and consequent reduction in the buoyancy. For higher Grashof numbers, a slightly sharper decrease in $v^*_{in,nc}$ can be seen during a range of intermediate Reynolds numbers. This range is about 200–300 for $Gr = 5 \times 10^6$ and 300–400 for $Gr = 10^7$. However, such a trend of $v^*_{in,nc}$ with Re is not observed for lower Grashof numbers. Fig. 5 shows that the natural convection induced velocity tends to stabilise at a finite value with increase in the Reynolds number. This can be clearly seen in the case of lower Grashof numbers for which $v^*_{in,nc}$ has already reached nearly a constant value at a Reynolds number of about 900.

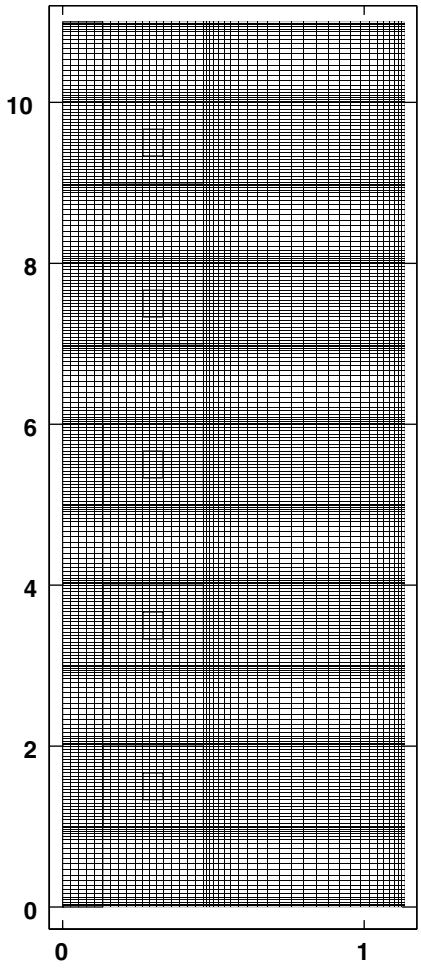

Fig. 4. Grid point distribution in the 45×259 mesh.

Table 3
Dimensionless pressure drop across the channel for various Reynolds numbers

Re	Δp^+	Re	Δp^+	Re	Δp^+
10	36.835	200	3.2794	900	1.8490
20	19.041	300	2.7097	1000	1.7991
30	13.148	400	2.4074	1100	1.7574
40	10.175	500	2.2158	1200	1.7224
50	8.4074	600	2.0816	1300	1.6925
75	6.0677	700	1.9820	1400	1.6668
100	4.9269	800	1.9102	1500	1.6443

Note: $\Delta p^* = \Delta p^+ Re^2$.

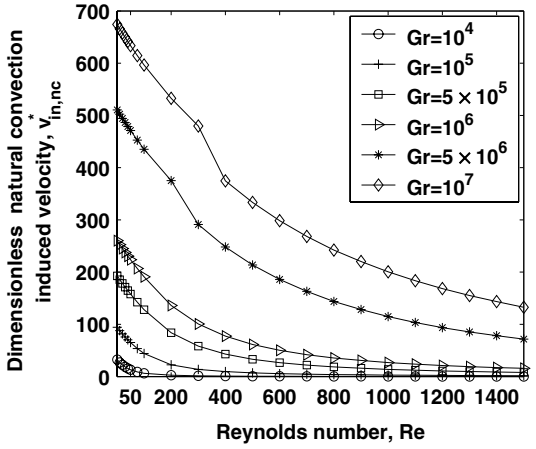

Fig. 5. Variation of the dimensionless natural convection induced velocity at the channel inlet with Reynolds number for various Grashof numbers.

In obtaining a correlation for the natural convection induced velocity, first two separate correlations fitting the lower and higher ends of the chosen Reynolds number range are obtained. The following composite correlation spanning the complete range of Reynolds number is then constructed obtaining guidance from the work of Churchill [31]:

$$v^*_{\mathrm{in,nc}} = \left[\left[0.7744Gr^{0.42} - 0.7Re + 0.2526Gr^{-0.42}Re^2\right]^{\frac{1}{n}} + \left[\frac{104.04 + 0.2631Gr^{0.84}}{Re}\right]^{\frac{1}{n}}\right]^n \quad (11)$$

where $n = -5$. The range of validity of the above correlation is $0 \leqslant Re \leqslant 1500$ and $10^4 \leqslant Gr \leqslant 10^7$. For the above correlation, the multiple correlation R^2, defined as $1 -$ (mean square error)/(variance), is found to be 0.98. The pure natural convection induced velocity can be predicted with a slightly better accuracy with the following correlation ($R^2 = 0.987$), rather than by setting $Re = 0$ in Eq. (11):

$$v^*_{\mathrm{in,pnc}} = 0.59Gr^{0.44} \quad (12)$$

4.2. Streamline and isotherm maps

The stream function is defined by a line integral as follows:

$$\psi^* = \psi^*_{\mathrm{ref}} + \int (u^*\,\mathrm{d}y^* - v^*\,\mathrm{d}x^*) \quad (13)$$

where ψ^*_{ref} is taken as zero on the left solid–fluid interface. The flow distribution is depicted by means of selected streamline maps. In the case of forced and mixed convection cases, the stream function values are normalised with the Reynolds number. Fig. 6 shows the streamlines for $Re = 200$ and 1500 with $Gr = 0$ (i.e., pure forced convection). From these figures, it can be seen that at higher Reynolds numbers, the stagnation points inside the inter-

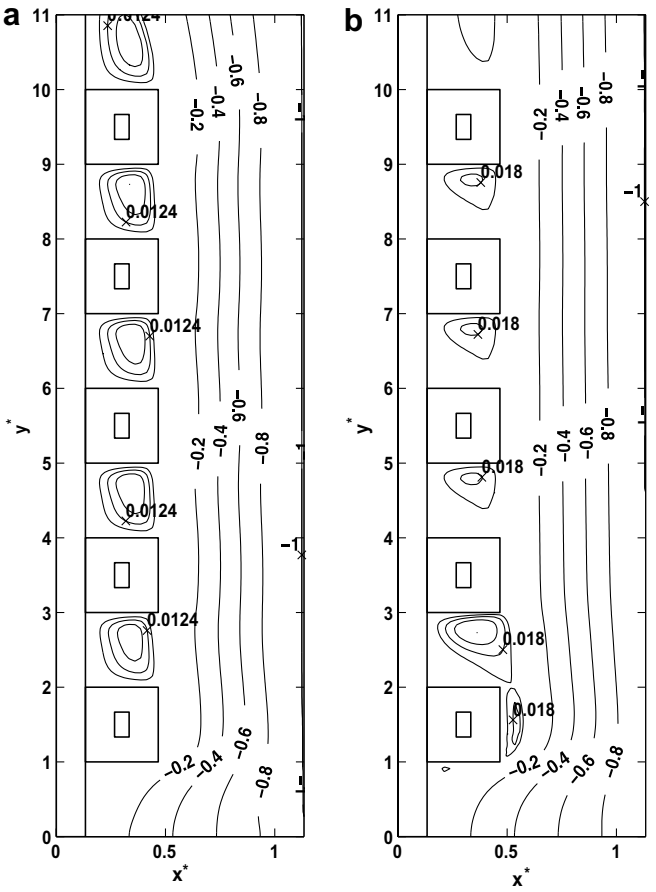

Fig. 6. Streamlines for pure forced convection. (a) $Re = 200$, (b) $Re = 1500$ (the stream function values are normalised with Reynolds number).

component circulations tend to move towards the bottom faces of the components. There is also a tendency for the appearance of an additional vortex adjacent to the right face of the bottom-most component. Fig. 7 shows the streamline maps for $Re = 0$ (i.e., pure natural convection) for $Gr = 10^5$ and 5×10^6. For the lower Grashof number, the recirculations in the regions between the blocks are weak with the stagnation point lying nearer to the upper faces of the blocks. At the higher Grashof number, the inter-block eddies are pressed towards the lower faces of the components. An important difference in the flow field between the forced and free convection is that in the former case the flow appears to exit the channel in an upward direction while in the latter case a deflection of the streamlines to the left side occurs at the exit of the channel. The streamline maps for forced convection ($Gr = 0$) and mixed convection ($Gr = 10^5$, 10^6 and 5×10^6) are shown in Fig. 8 for $Re = 200$. The changes in the fluid circulation with increasing Grashof number at this Reynolds number are similar to those for pure natural convection.

The temperature distribution in the channel is depicted by selected isotherm maps in Fig. 9 for $Re = 200$ and various Grashof numbers. It can be seen from this figure that

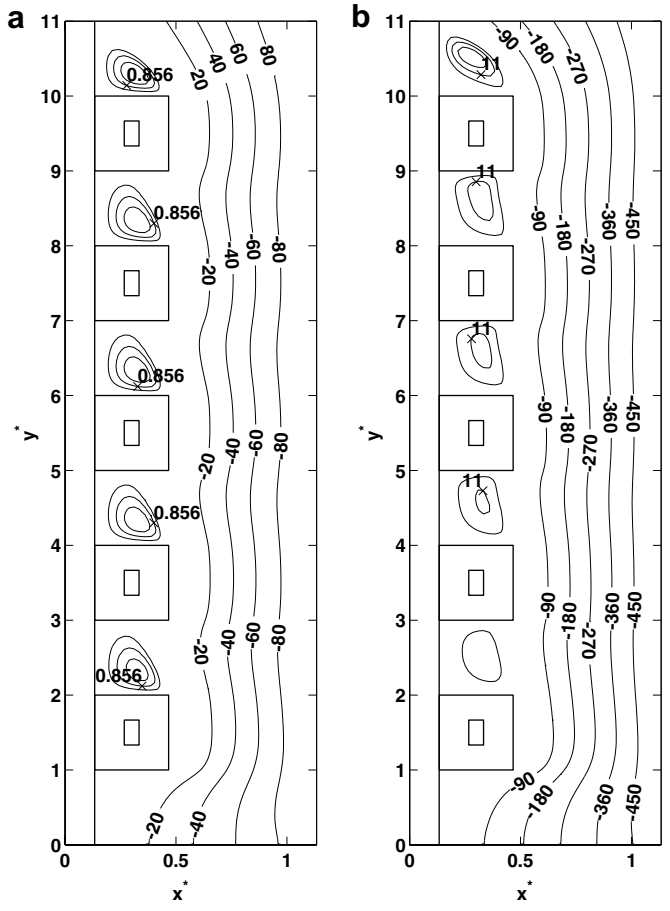

Fig. 7. Streamlines for pure natural convection. (a) $Gr = 10^5$, (b) $Gr = 5 \times 10^6$.

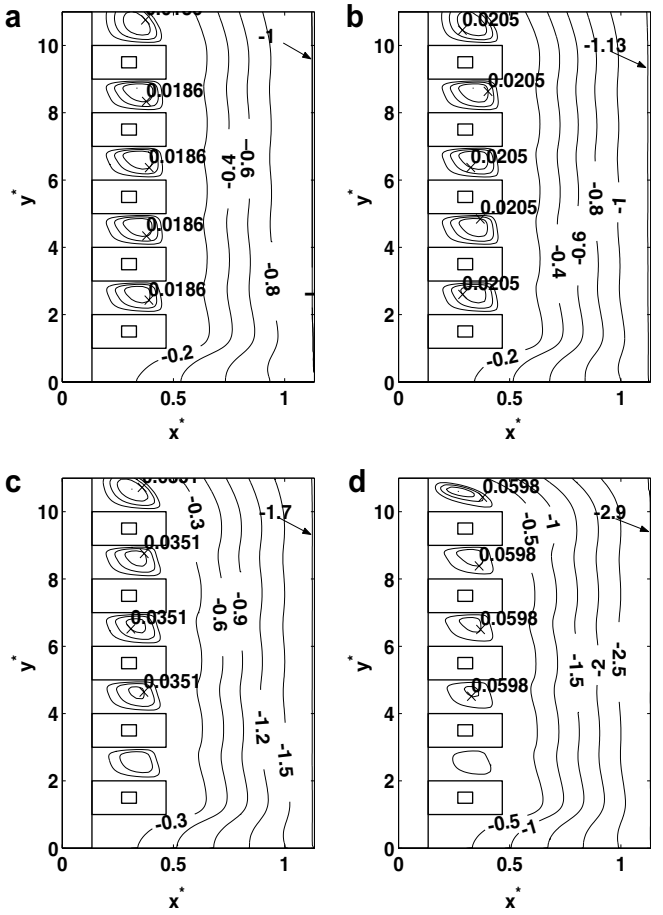

Fig. 8. Streamlines for a Reynolds number of 200. (a) $Gr = 0$, (b) $Gr = 10^5$, (c) $Gr = 10^6$, (d) $Gr = 5 \times 10^6$ (the steam function values are normalised with Reynolds number).

the temperature distribution inside any package is typical to the case where volumetric heat generation is present, i.e., closed isotherms with the heat generated being conducted down the gradient. For higher Grashof numbers, namely, 5×10^5 and 10^6, more homogenisation of temperature takes place in the heat source region of the package. As the Grashof number increases, the penetration depth of the thermal effects into the core fluid from the left side packages and from the right side substrate surface decreases due to higher velocities. The values of the dimensionless temperature decrease with increasing Grashof number only because the quantity $T - T_{\text{in}}$ increases at a smaller rate compared to the heat rate $\dot{Q}_{\text{L}}$. The dimensional temperatures, however, increase with increasing Grashof number. The temperature distributions for the pure forced and natural convection cases are not shown because they are qualitatively similar to the mixed convection case.

It may be noted that in view of the larger height to width ratio of the channel, the aspect ratio is not maintained in the contour maps.

4.3. Dimensionless solid–fluid interface temperature

The dimensionless temperature of the left solid–fluid interface is shown in Fig. 10 for Grashof numbers 0, 10^5, 10^6 and 5×10^6. For each Grashof number, the variation of the interface temperature is shown for various Reynolds numbers (100, 400, 800 and 1200). With increasing distance along the interface starting from the bottom of the channel, the temperature on the whole increases, saving for the dips in the substrate regions and weak local extrema in the component regions. This is due to the heating of the working fluid as it moves up the channel. The component at the end of the channel registers in general the highest temperature. Closer examination reveals that the anticlockwise eddy in the inter-component spacing has the effect of lowering the block bottom face temperature as the right corner is approached from the substrate end. The eddy, however, has a less pronounced effect on the temperature of the upper face of the block. The temperature of the vertical face of the block adjacent to the fluid shows a local maximum because of the presence of the heat source inside the package. The substrate appears to have good heat redistribution capability due to its finite thickness. Increasing Reynolds number has the effect of reducing temperatures at various locations on the interface. The dimensionless interface temperatures can be seen to decrease with increasing Grashof number, but this will actually be an increase when it comes to dimensional temperature.

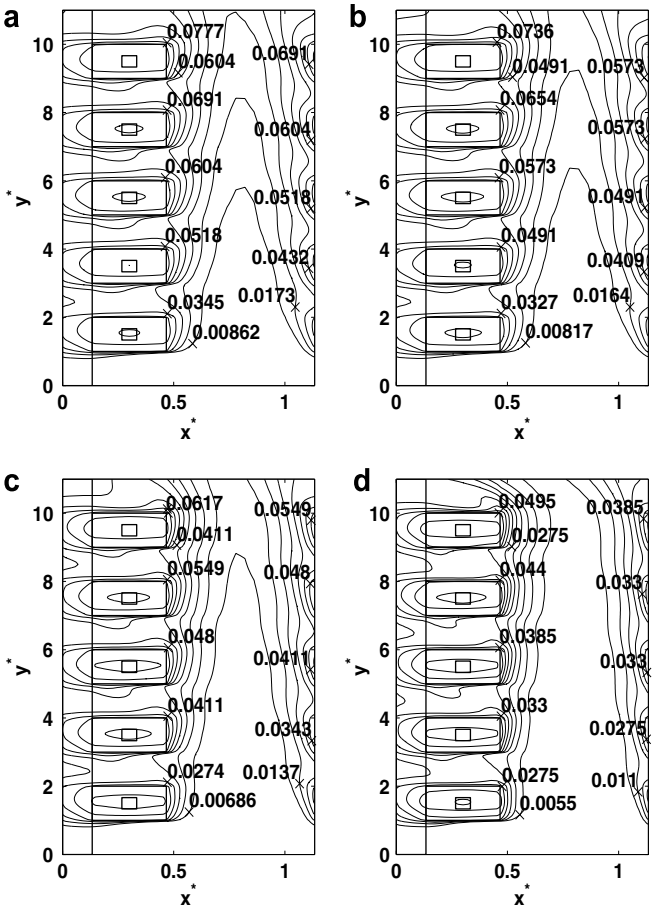

Fig. 9. Isotherms for a Reynolds number of 200. (a) $Gr = 0$, (b) $Gr = 10^5$, (c) $Gr = 10^6$, (d) $Gr = 5 \times 10^6$.

4.4. Local Nusselt number along the solid–fluid interfaces

The variation of the local Nusselt number $Nu_{l,l}$ along the left solid–fluid interface inside the channel is shown in Fig. 11. It can be seen from this figure that at any Grashof number, the gap regions between the packages can result in small but negative local Nusselt numbers. The reason can be traced to the fact that a substantial heat transfer takes place from the horizontal surfaces of the packages into the fluid recirculating in the inter-rib spacing. It may be noted that the package thermal conductivity ratio is 10 times that of the substrate. In view of this, there is a temperature gradient across the thickness of the substrate favouring heat transfer from the inter-rib spacing into the fluid flowing on the other side of the substrate, although for the chosen parameters this heat transfer is very small, as already mentioned. The larger temperature dips on the left solid–fluid interface in the inter-rib spacings can also be attributed to this behaviour.

Moreover, while the local Nusselt number along the bottom face of the component increases, it decreases along the vertical and the upper faces. Barring the substrate region at the channel inlet, the module-to-module variation of the local Nusselt number becomes almost the same for the rest of the channel. At a corner, a local Nusselt number can be defined in either direction. In view of this, discontinuities in the local Nusselt number can be seen at the various corners. It can be seen that the trend of the local Nusselt number is similar in both pure natural convection and mixed convection cases.

The variation of the local Nusselt number $Nu_{l,r}$ for the right solid–fluid interface is shown in Fig. 12. It can be seen from this figure that the local Nusselt number variation along the right solid–fluid interface is undulatory with local maxima occurring in the regions adjacent to the blocks and local minima in the regions adjacent to inter-component spaces. The local Nusselt number $Nu_{l,r}$ is much higher at the entrance and decreases sharply within a small distance downstream. This behaviour can be attributed to the fact that $Nu_{l,r}$ is directly proportional to the heat flux and inversely proportional to the surface temperature. If the right solid–fluid interface is imagined to be composed of segments each spanning the center-to-center distance of the packages, it can be seen that the corresponding locations of the segments show progressively lower local Nusselt numbers, but the trend downstream is a gradual and almost linear decrease. The effect of increasing Reynolds number at any given Grashof number is to increase $Nu_{l,r}$ at any location. A comparison of the subfigures shows that an increase in Grashof number tends to improve the value of $Nu_{l,r}$. However, it can be seen that the improvement in $Nu_{l,r}$ with increasing Reynolds number decreases at higher Grashof numbers.

4.5. Maximum dimensionless temperature

Fig. 13 shows the variation of the maximum dimensionless temperature with Reynolds number for various Grashof numbers. In the channel, local temperature maxima occur inside each package. The maximum dimensionless temperature T^*_{max} referred to here is the maximum of the local maxima and occurs in the heat source of the package located at the channel exit. The curves for the different Grashof numbers are seen to merge with that of the pure forced convection beyond a Reynolds number of 1000, indicating the threshold of the region of forced convection dominance. Thus the results show that in the range of Reynolds number between 0 and 1000, the assumption of either pure natural convection or pure forced convection can lead to inaccuracies in the prediction of the maximum temperature. Although the dimensionless maximum temperature decreases with increasing Grashof number, it should be noted that the dimensional temperature actually increases, because for fixed geometrical parameters and a given heat transfer medium, an increase in Grashof number means an increase in the heat generation. This can be seen from Fig. 14, where the maximum dimensional temperature is plotted against the fan velocity for a channel geometrically similar to that shown in Fig. 1 with width $W_c = 30$ mm, for an inlet air temperature of 25 °C. The power ratings shown are for packages each of breadth, height and width 30 mm,

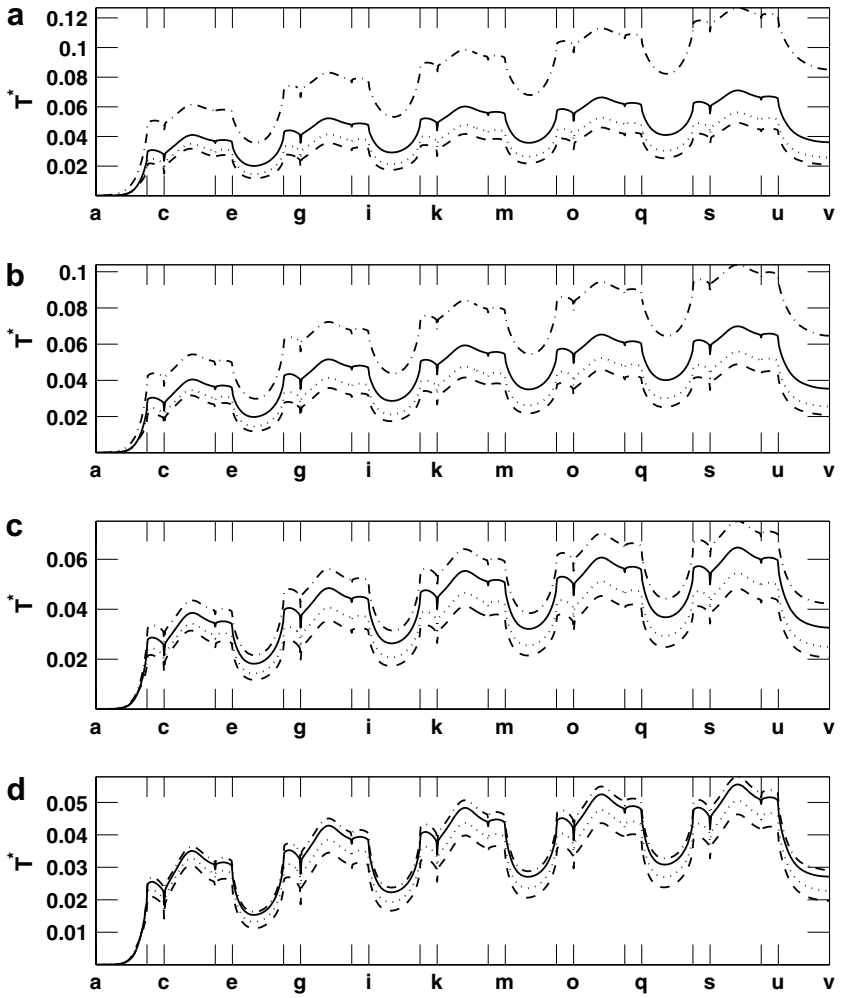

Fig. 10. Variation of the dimensionless temperature along the left solid–fluid interface. Dot-dash line: $Re = 100$. Continuous line: $Re = 400$. Dotted line: $Re = 800$. Dashed line: $Re = 1200$. (a)$Gr = 0$, (b) $Gr = 10^5$, (c) $Gr = 10^6$, (d) $Gr = 5 \times 10^6$.

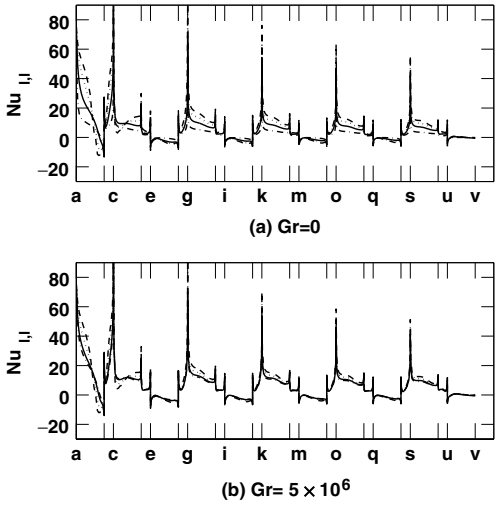

Fig. 11. Variation of the local Nusselt number along the left solid–fluid interface. Dot-dash line: $Re = 100$. Continuous line: $Re = 400$. Dotted line: $Re = 800$. Dashed line: $Re = 1200$. (a) $Gr = 0$, (b) $Gr = 5 \times 10^6$.

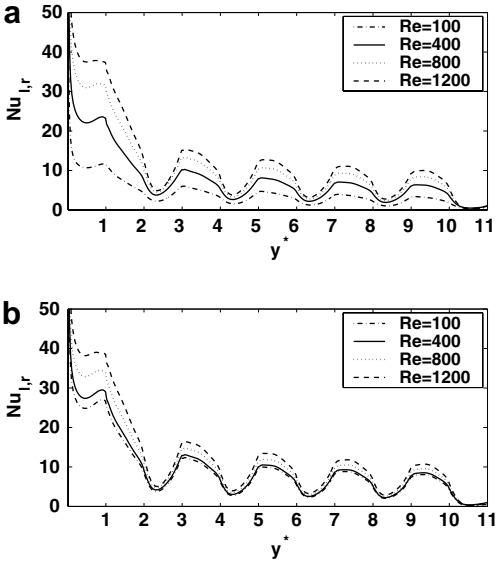

Fig. 12. Variation of the local Nusselt number along the right solid–fluid interface. (a) $Gr = 0$, (b) $Gr = 5 \times 10^6$.

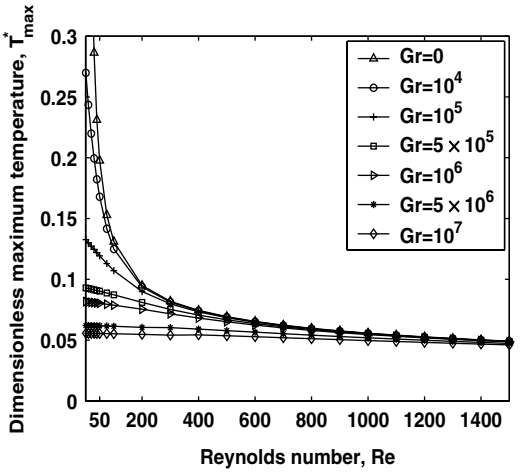

Fig. 13. Variation of the maximum dimensionless temperature with Reynolds number for various Grashof numbers.

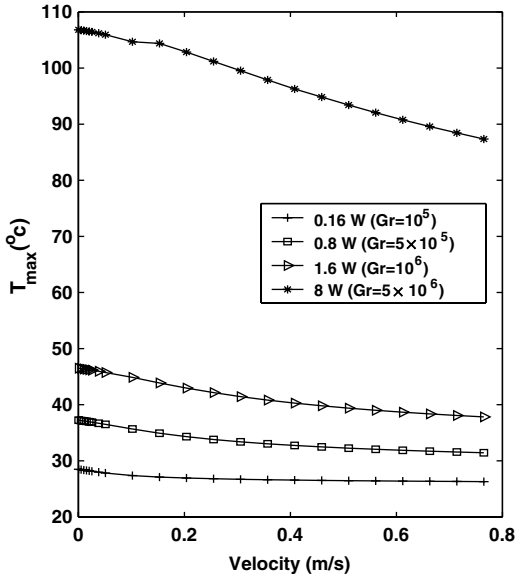

Fig. 14. Variation of the maximum dimensional temperature with forced velocity for various power ratings of the packages (breadth, height and width of each package: 30 mm × 30 mm × 10 mm) for an inlet air temperature of 25 °C.

30 mm and 10 mm. In view of the two-dimensional approximation, the packages are assumed to be arranged without any spacing between them in the third direction. The temperatures obtained for $Gr \geqslant 5 \times 10^6$, for the chosen dimensions, should be considered as an approximation because at such high temperatures, the Boussinésq approximation can become inadequate.

The pure natural convection correlation for T^*_{max} for the range $10^4 \leqslant Gr \leqslant 5 \times 10^6$ is found to be

$$T^*_{max} = 2.21 Gr^{-0.24} \tag{14}$$

Including the data for $Gr = 10^7$ also, the correlation obtained is

$$T^*_{max} = 1.92 Gr^{-0.22} \tag{15}$$

For the pure forced convection case ($10 \leqslant Re \leqslant 1500$) the correlation is

$$T^*_{max} = 1.49 Re^{-0.48} \tag{16}$$

It may be noted that the exponent on Grashof number in Eq. (14) is twice that on Reynolds number in Eq. (16). However, with the forced convection and natural convection asymptotes chosen respectively as $(1/T^*_{max})/Re^{0.48} = 0.671$ and $(1/T^*_{max})/Re^{0.48} = 0.452 Ar^{0.24}$ (where $Ar = Gr/Re^2$ is the Archimedes or the Richardson number), when the quantity $(1/T^*_{max})/Re^{0.48}$ for the complete data is plotted against $Ar^{0.24}$ along with the natural and forced convection asymptotes, the merging of the data with the forced convection asymptote is not found to be satisfactory.

Reexamination of the data revealed that a composite correlation for $1/T^*_{max}$ can be constructed in terms of the natural convection and forced convection inlet velocity asymptotes. The correlation for pure natural convection induced velocity for the range $10^4 \leqslant Gr \leqslant 10^7$ is given by Eq. (12). The relation for T^*_{max} in terms of $v^*_{in,pnc}$ is

$$T^*_{max} = 1.46 v^{*-0.51}_{in,pnc} \tag{17}$$

The forced convection and natural convection asymptotes are thus $(1/T^*_{max})/Re^{0.48} = 0.67$ and $(1/T^*_{max})/Re^{0.48} = 0.68 v^{*0.51}_{in,nc}/Re^{0.48}$. If the exponents of $v^*_{in,nc}$ and Re are rounded to 0.5 (nearest first decimal place), it is found to be satisfactory to take forced and natural convection asymptotes as $(1/T^*_{max})/Re^{0.5} = 0.63$ and $(1/T^*_{max})/Re^{0.5} = 0.7(v^*_{in,nc}/Re)^{0.5}$, respectively. In terms of these asymptotes, the following composite correlation can be presented using the method of Churchill [31]:

$$\frac{1}{T^*_{max}} = Re^{0.5}\left\{0.63^n + \left(0.7\frac{v^*_{in,nc}}{Re}\right)^{0.5n}\right\}^{1/n} \tag{18}$$

With n chosen as 3/2, the complete data fits the above correlation with an R^2 value of 0.9984. The ranges of validity for the above correlation are $10^4 \leqslant Gr \leqslant 10^7$ and $10 \leqslant Re \leqslant 1500$. The agreement between the computed data and the correlation is shown in Fig. 15, from which the mixed convection régime can be seen to span the range $0.2 < \left(v^*_{in,nc}/Re\right)^{0.5} < 5$. The correlation is based on 132 computed data points.

4.6. Substrate heat conduction

The effect of substrate heat conduction is shown in Fig. 16. From this figure, it can be clearly seen that the heat removal through substrate heat conduction accounts for as high as 41–47% of the total heat generated in the components over the parameter range considered, with the higher value occurring at lower Grashof numbers for a fixed Reynolds number. From this result it can be stated that simple analyses with isothermal and isoflux boundary conditions are not appropriate and that even a lower thermal conduc-

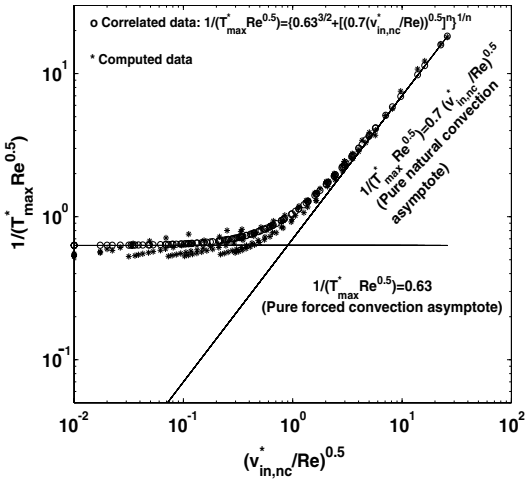

Fig. 15. Plot of computed and correlated data for dimensionless maximum temperature with asymptotes based on pure natural convection induced inlet velocity and Reynolds number.

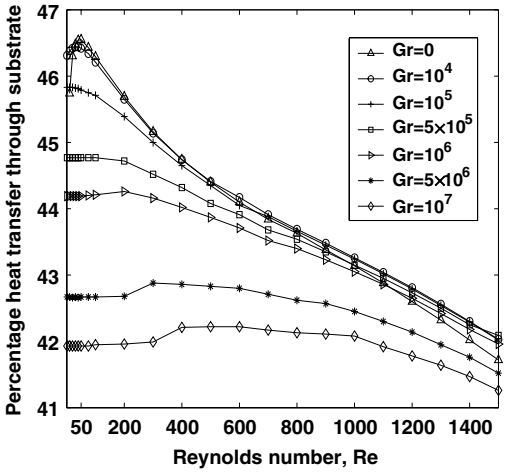

Fig. 16. Variation of the percentage heat transfer through the substrate with Reynolds number for various Grashof numbers.

tivity substrate can be very effective in heat removal and in redistributing the heat from the components. However, the heat removed by substrate heat conduction is also ultimately transferred to the fluid from the smooth surface of the substrate.

4.7. Average Nusselt numbers

The average Nusselt number $Nu_{a,l}$ based on the maximum temperature is shown Fig. 17. It can be seen that $Nu_{a,l}$ has a variation which is roughly the opposite of T^*_{max}. However, $Nu_{a,l}$ is not proportional to $1/T^*_{max}$. This is because the entire heat generated is not dissipated through the left solid–fluid interface alone; some of it is conducted across the substrate and is dissipated from the smooth surface of the substrate (right solid–fluid interface). The variation of the average Nusselt number $Nu_{a,r}$ of the right solid–fluid interface is found to be similar to that of $Nu_{a,l}$.

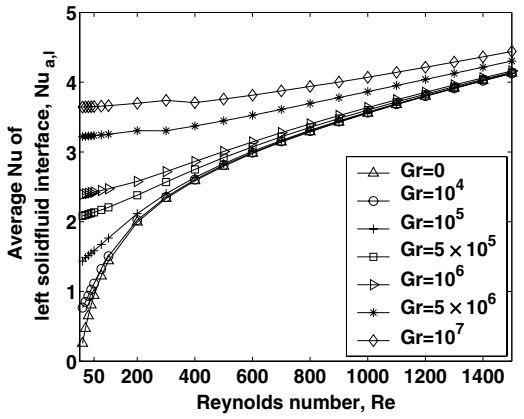

Fig. 17. Variation of the average Nusselt number (based on the maximum temperature) of the left solid–fluid interface with Reynolds number for various Grashof numbers.

5. Conclusions

Two-dimensional, laminar, natural, forced and mixed convective heat transfer from protruding volumic heat sources attached to vertical substrates forming a series of channels is studied numerically by selecting a representative domain with periodic thermal boundary conditions in the transverse direction. The heat sources and substrates simulate integrated circuit packages attached to printed circuit boards. The Reynolds number is based on the fan velocity component rather than the combined natural and forced convection velocity. The velocity induced by natural convection in the mixed convection situation is found by assuming that the mixed and forced convection pressure drops through the channel are the same for a given Reynolds number. At a given Grashof number, the natural convection induced velocity component in the presence of mixed convection decreases with increasing Reynolds number due to better cooling of the components and consequent reduction in the buoyancy. The maximum dimensionless temperature approaches the forced convection value for Reynolds numbers more than about 1000 for different Grashof numbers. In the range of Reynolds number between 0 and 1000, the assumption of either pure natural convection or pure forced convection can lead to inaccuracies in the prediction of the maximum temperature. The heat removal by substrate heat conduction accounts for as high as 41–47% of the total heat generated in the components over the parameter range considered. The results show that simple adiabatic boundary condition for the substrate and isothermal or isoflux condition for the heat source portions are not appropriate and that the conjugate nature of the problem should be duly considered taking into account the heat conduction in both the components and the substrate. Even a lower thermal conductivity substrate can be very effective in terms of heat removal and redistribution of the heat from the components. Correlations are obtained for the prediction of the natural convection induced velocity in terms of the Grashof and

Reynolds numbers. The maximum dimensionless temperature is correlated in terms of pure natural convection and forced convection inlet velocity asymptotes for fixed geometrical parameters and Prandtl number corresponding to that of air.

References

[1] L. Graetz, Ueber die Wärmeleitungsfähigkeit von Flussigkeiten, Ann. Phys. Chem., Part 1 (18) (1883) 79–94;
L. Graetz, Ueber die Wärmeleitungsfähigkeit von Flussigkeiten, Ann. Phys. Chem., Part 2 (25) (1885) 337–357.

[2] W. Elenbaas, Heat dissipation of parallel plates by free convection, Physica 9 (1) (1942) 1–28.

[3] S. Ostrach, Combined natural and forced convection laminar flow and heat transfer of fluids with and without heat sources in channels with linearly varying wall temperature, NACA TN 3141, 1954.

[4] R.K. Shah, A.L. London, in: T.F. Irvine, Jr., J.P. Hartnett (Eds.), Advances in Heat Transfer, Supplement 1, Laminar Flow Forced Convection in Ducts: A Source Book for Compact Heat Exchanger Analytical Data, Academic Press, New York, 1978.

[5] S. Ostrach, in: F.K. Moore (Ed.), High Speed Aerodynamics and Jet Propulsion, Laminar flows with body forces, Section F, Theory of Laminar Flows, vol. IV, Princeton University Press, Princeton, New Jersey, 1964, pp. 528–718.

[6] G.D. Raithby, K.G.T. Hollands, in: W.M. Rohsenow, J.P. Hartnett, E.N. Ganić (Eds.), Handbook of Heat Transfer Fundamentals, Natural Convection, Section 6, second ed., McGraw-Hill Book Co., New York, 1985, pp. 6-1–6-94.

[7] W. Aung, in: S. Kakaç, R.K. Shah, W. Aung (Eds.), Handbook of Single Phase Convective Heat Transfer, Mixed Convection in Internal Flow, Section 15, John Wiley & Sons, New York, 1987, pp. 15-1–15-55.

[8] W. Nakayama, Thermal management of electronic equipment: research needs in the mid-1990s and beyond, Appl. Mech. Rev., Part 2 49 (10) (1996) S167–S174.

[9] J. Davalath, Y. Bayazitoglu, Forced convection cooling across rectangular blocks, ASME J. Heat Transfer 109 (1987) 321–338.

[10] I.J. Young, K. Vafai, Experimental and numerical investigation of forced convective characteristics of array of channel mounted obstacles, ASME J. Heat Transfer 121 (1999) 34–42.

[11] H.Y. Wang, J.B. Saulnier, A sensitivity study of material properties for coupled convective–conductive heat transfer generated in an electronic equipment, Int. J. Heat Mass Transfer 36 (15) (1993) 3831–3839.

[12] S.H. Kim, N.K. Anand, Laminar developing flow and heat transfer between a series of parallel plates with surface mounted discrete heat sources, Int. J. Heat Mass Transfer 37 (15) (1994) 2231–2244.

[13] S.H. Kim, N.K. Anand, Laminar heat transfer between a series of parallel plates with surface-mounted discrete heat sources, ASME J. Heat Transfer 117 (1995) 52–62.

[14] Y. Asako, M. Faghri, Three-dimensional heat transfer analysis of arrays of heated square blocks, Int. J. Heat Mass Transfer 32 (2) (1989) 395–405.

[15] Y. Joshi, T. Wilson, S.J. Hazard III, An experimental study of natural convection cooling of an array of heated protrusions in a vertical channel in water, ASME J. Electron. Pack. 111 (1989) 33–40.

[16] H.Y. Wang, F. Penot, J.B. Sauliner, Numerical study of a buoyancy induced flow along a vertical plate with discretely heated integrated circuit packages, Int. J. Heat Mass Transfer 40 (1997) 1509–1520.

[17] S.Y. Kim, H.J. Sung, J.M. Hyun, Mixed convection from multiple-layered boards with cross-streamwise periodic boundary conditions, Int. J. Heat Mass Transfer 35 (11) (1992) 2941–2952.

[18] J.C. Watson, N.K. Anand, L.S. Fletcher, Mixed convective heat transfer between a series of vertical parallel plates with planar sources, ASME J. Heat Transfer 118 (1996) 984–990.

[19] M. Najam, A. Amahmid, M. Hasnaoui, M.E. Alami, Unsteady mixed convection in a horizontal channel with rectangular blocks periodically distributed on its lower wall, Int. J. Heat Fluid Flow 24 (2003) 726–735.

[20] C.G. Rao, C. Balaji, S.P. Venkateshan, Effect of radiation on conjugate mixed convection in a vertical channel with a discrete heat source in each wall, Int. J. Heat Mass Transfer 45 (2002) 3331–3347.

[21] G.I. Sultan, Enhancing forced convection heat transfer from multiple protruding heat sources simulating electronic components in a horizontal channel by passive cooling, Microelectron. J. 31 (2000) 773–779.

[22] Q. Wang, Y. Jaluria, Unsteady mixed convection in a horizontal channel with protruding heated blocks and a rectangular vortex promoter, Phys. Fluids 14 (7) (2002) 2113–2127.

[23] M.E. Braaten, S.V. Patankar, Analysis of laminar mixed convection in shrouded arrays of heated rectangular blocks, Int. J. Heat Mass Transfer 28 (9) (1985) 1699–1709.

[24] A.M. Dalbert, Natural, mixed and forced convection in a vertical channel with asymmetric uniform heating, Heat Transfer 1982: Proc. Seventh Int. Heat Transfer Conf., München, vol. 3, Hemisphere Publishing Corporation, Washington, 1982, pp. 431–434.

[25] W. Shyy, in: J.P. Hartnett, T.F. IrvineJr., Y.I. Cho (Eds.), Advances in Heat Transfer, Elements of Pressure-based Computational Algorithms for Complex Fluid Flow and Heat Transfer, vol. 24, Academic Press, Boston, 1994, pp. 191–275.

[26] K.J. Kennedy, A. Zebib, Combined forced and free convection between parallel plates, Heat Transfer 1982: Proc. Seventh Int. Heat Transfer Conf., München, vol. 3, Hemisphere Publishing Corporation, Washington, 1982, pp. 447–451.

[27] S.V. Patankar, Numerical Heat Transfer and Fluid Flow, McGraw-Hill, New York, 1980.

[28] G. de Vahl Davis, Natural convection of air in a square cavity: a bench mark numerical solution, Int. J. Numer. Methods Fluids 3 (1983) 249–264.

[29] D.C. Wan, B.S.V. Patnaik, G.W. Wei, A new benchmark quality solution for the buoyancy-driven cavity by discrete singular convolution, Numer. Heat Transfer, Part B: Fundamen. 40 (2001) 199–228.

[30] C.Y. Choi, A. Ortega, Mixed convection in an inclined channel with discrete heat sources, Int. J. Heat Mass Transfer 36 (1993) 3119–3134.

[31] S.W. Churchill, The Interpretation of and Use of Rate Data: The Rate Concept, Scripta/McGraw-Hill, Washington, DC/New York, 1974.